

Synthesis of boron nanoparticles by a hybrid “polyol-solvothermal” process using glycerol as reducing agent

A. Casas Mendoza^a, A. García Murillo^{a,*}, F. de J. Carrillo Romo^a, and J. Ortíz Landeros^b

^a*Instituto Politécnico Nacional, Centro de Investigación e Innovación Científica, Cerrada de Cecati s/n, Azcapotzalco, Santa Catarina, CDMX, 02250, México.*

**e-mail: angarciam@ipn.mx*

^b*Instituto Politécnico Nacional-ESIQIE, Av. Instituto Politécnico Nacional s/n. CDMX, 07738, México.*

Received 5 June 2024; accepted 30 October 2024

In this article, a novel hybrid synthesis process called the “polyol-solvothermal process” is presented. This process utilizes a polyol-solvothermal hybrid method under acidic conditions (pH= 1) to obtain amorphous boron nanoparticles with a spherical morphology. The synthesis parameters include different concentrations of metalloid ions (1 and 2 M), glycerol (50% and 80% w/w), and PVP (0.01 g and 0.02 g). To examine the morphology and particle size, surface plasmon resonance (SPR), transmission electron microscopy (TEM), and scanning electron microscopy (SEM) were employed. The TEM analysis revealed the presence of spherical nanoparticles with an average size of ~ 5 nm and quasi-spherical microparticles with an average diameter of 3.5 micrometers. This suggests the presence of microparticles composed of smaller particles, which was confirmed by the surface plasmon resonance (SPR) results. The SPR analysis revealed bands around 275 nm, indicating the presence of boron nanoparticles. The X-ray diffraction (XRD) results show a single peak associated with the formation of amorphous boron. Furthermore, the FT-IR studies identified a peak between 1019 and 1040 cm^{-1} , which is related to the stretching vibrational bond of $\text{CH}_2\text{-OH}$, indicating the decomposition of glycerol into primary alcohols, which acted as reducing agents. Another band, located at approximately 500 cm^{-1} and characteristic of the M-O vibrational bond, was associated with the formation of metal nanoparticles.

Keywords: Green synthesis; glycerol; hybrid method; boron; nanoparticle.

DOI: <https://doi.org/10.31349/RevMexFis.71.021003>

1. Introduction

Metallic and metalloid nanoparticles are of great interest, due to their optical [1], catalytic [2], electrical [3], magnetic [4], biological [5], and energetic properties [6]. Some of these properties are shared by certain metalloids, such as boron [7]. However, despite belonging to the semiconductor family, boron exhibits a high energy density (137.7 MJ/Kg), making it particularly intriguing to the field of highly energetic materials.

The properties of metallic and metalloid nanoparticles are closely linked to their synthesis processes [8]. There are a few reports on the synthesis of micro- and nanoparticles by physical techniques, including condensation and evaporation [9], laser ablation [10], pyrolysis [11], and high-energy ball milling [12]. However, these approaches suffer from several drawbacks. They often yield a low quantity of nanoparticles, are expensive, and consume substantial amounts of energy. Additionally, they lack control over particle size and morphology, and they typically require the use of toxic reducing agents, such as sodium boron hydride (NaBH_4), hydrazine, and potassium bitartrate, posing risks to human health and the environment [13]. In contrast, chemical processes like chemical reduction [14], hydrothermal synthesis [15], and sol-gel methods [16] offer several advantages. They do not require complex equipment for synthesis and, depending on

the conditions, can yield metal and metalloid nanoparticles with a well-defined morphology, controlled particle size, and high purity [17]. So far there are no reports on the synthesis of micro- and nanoparticles of metalloids such as boron, using glycerol as reducing agent. Hence, the current study describes a novel route through a “polyol-solvothermal” hybrid process that uses borax as a precursor of the metal ions and glycerol as reducing agent.

In recent years, the excessive burning of fossil fuels and growing concerns over environmental preservation have led to a significant increase in the worldwide consumption of biodiesel. Consequently, industries dedicated to the production of this eco-friendly fuel have experienced a surge in demand [18]. Glycerol is generated, with a yield of 100 kg per ton of refined biodiesel [19]. In the food and cosmetics industries, glycerol has found various applications as a non-toxic chemical component in the production of food and makeup products [20]. Recently, due to its chemical properties, it has gained interest as a substance with potential use in the synthesis of micro- and nanomaterials, where it can serve as a chemical agent, replacing organic solvents derived from petroleum and functioning as both a reducing agent and a stabilizing agent in the synthesis of noble metal nanoparticles [21]. Through three different processes [22], it can reduce metal cations: (a) catalytic reduction, (b) reduction by aldehydes, and (c) reduction by alkoxides.

As a chemical agent, glycerol poses no risk to the human body, animals, or the environment [23]. It possesses several important characteristics for the synthesis of metal nanoparticles, including (a) high pressure at high temperatures, (b) decomposition into primary alcohols and radicals (which reduce metal ions to a 0 valence) at temperatures above its melting point (290°C), and (c) an electrical permittivity ($\epsilon = 42.3$) similar to that of water, as well as a density of 1.261 gcm^{-3} , which makes it a suitable solvent for organic compounds and inorganic salts, based on their optical, conductive, catalytic, and microbial properties. Metal nanoparticles (such as Au, Pt, Fe, and Ag) and metal oxides (CuO, ZrO₂, and MgO) have been successfully obtained through synthesis processes that involve the use of glycerol as a reducing agent under different conditions involving pressure, temperature, pH, and metal ion concentration. Commonly used synthesis methods include chemical reduction [24], hydrothermal synthesis [25], the sol-gel method [26], and microwave irradiation [27], which play a vital role in the formation of cell walls in plants due to their influence on the prebiotic metabolic cycle involving formaldehyde [28]. As a light element, it has been utilized for various applications in protective coatings [29], refractory materials [30], semiconductors [31], and metallic fuels [32]. Boron can come in two different structural arrangements: crystalline and amorphous. α -Rhombohedral (α -R), β -rhombohedral (β -R), and β -tetragonal (β -T) are the most stable; this is due to a well-defined structure that has stable thermal and electrical properties. However, amorphous boron can be a solid glass or fine powder. In both cases, the thermal and electrical properties are better because an atomic arrangement allows better flow between electrons and heat, and it has exceptional mechanical properties, making it suitable for use in coatings that can reduce fractures when amorphous boron has a sheet-like morphology [33]. Given the scarcity of reports (primarily through physical methods) on synthesizing boron micro- and nanoparticles, there are currently no reports covering the production of micro- and nanoparticles of metalloids like boron using glycerol as reducing agent and employing a “hybrid” chemistry process [34,35]. Moreover, to the best of our knowledge, there are no reports documenting the production of boron nanoparticles with a “polyol-solvothermal” methodology. The current study introduces a novel approach using a hybrid process, in which borax serves as a precursor for the metal ions, glycerol acts as a reducing agent, and PVP works as an encapsulant in an acidic medium (pH = 1) at a constant temperature of 250°C. The influence of glycerol and PVP concentrations on particle size and morphology under acidic conditions was investigated. The structural, morphological, and optical properties of boron nanoparticles were determined using X-ray diffraction (XRD), surface plasmon resonance (SPR), transmission electron microscopy (TEM), and scanning electron microscopy (SEM).

2. Experimental procedure

The reactants used for the hybrid polyol-solvothermal synthesis of boron nanoparticles, with glycerol as a reducing agent, were as follows: 99% glycerol (C₃H₈O₃) of commercial grade, sodium tetraborate (Na₂B₄O₇) (borax) (99%, Sigma Aldrich), polyvinylpyrrolidone (C₆H₉NO₉) (Fermont), and hydrochloric acid (HCl) 37%. All the reagents were used without prior treatment.

The conditions of synthesis and the labels for the boron nanoparticles - B-1, B-2, B-3, B-4, and B-5 - with the different concentration of glycerol, PVP, and metalloid ions are described in Table I.

The boron nanoparticles were prepared by a hybrid procedure. Figure 1 shows the first stage, which consisted of dissolving sodium tetraborate in 5 ml of deionized water to release boron ions ($Z=+3$) and polyvinylpyrrolidone (PVP).

Thereafter, 15 or 24 ml of glycerol were added dropwise to reduce the ions until 30 ml of a water/glycerol mixture was obtained, stirring constantly for 2 h. Subsequently, HCl was

TABLE I. Synthesis conditions and nomenclature of the boron nanoparticles.

Sample	Boron concentration (M)	Glycerol (%)	Polyvinylpyrrolidone (g)	pH
B-1	0.2	80		
B-2	0.1	80	0.02	
B-3	0.2	50		1
B-4	0.2	80		
B-5	0.1	50		

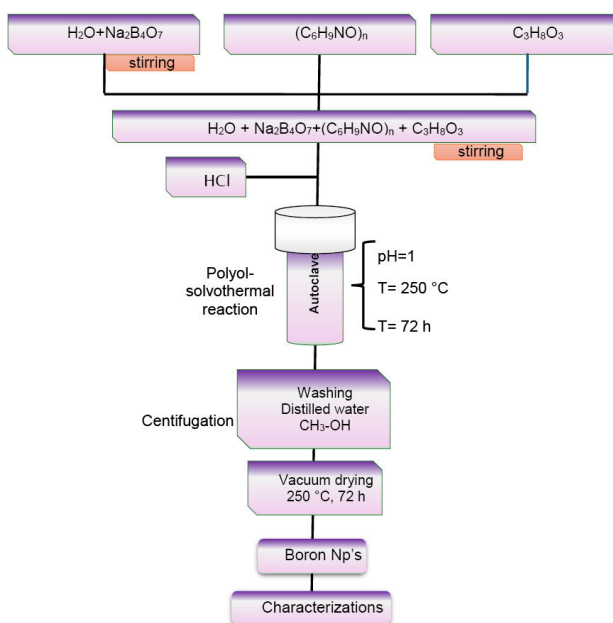


FIGURE 1. Synthesis of the boron nanoparticles using a hybrid “polyol-solvothermal” process.

added to produce a homogeneous and translucent solution of water, glycerol, sodium tetraborate, and PVP, with a pH = 1. The final solution of 30 ml was placed in a stainless-steel autoclave with a Teflon container and maintained at a temperature of 250°C for 72 h; these parameters were held constant because a slight change in any three parameters can modify the final pressure of the system causing changes on the final properties of boron nanoparticles.

The resulting powders were dark brown in color. They were washed several times with a solution of deionized water/methanol to remove impurities and dried inside a rotary evaporator with a chamber vacuum at 1 atm of pressure for 24 h. Finally, the powders were stored in a dry place at room temperature for later characterization.

3. Experimental techniques

X-ray diffraction (XRD) - on a Rigaku diffractometer (mini-flex600), within the range of 3° - 80° with a slit size of 0.6 mm and a step size of 0.02 has confirmed the formation of amorphous boron particles by the presence of a single broad peak located between 12° and 29°. The functional groups and decomposition mechanisms of glycerol were investigated in three different zones of the infrared spectrum. The results were analyzed using Fourier transform infrared spectroscopy with a Perkin Elmer Spectrum 65 FT-IR spectrometer. The size of the nanoparticles was studied using resonance plasmon spectroscopy (RPS) with an Agilent Cary Series UV-Vis-NIR spectrophotometer. Before morphological analysis, the boron nanoparticles were dispersed in ethanol under sonication for 5 min. A dispersion drop was placed on a copper grid, and characterization was performed using a JEOL Jem-2100 microscope.

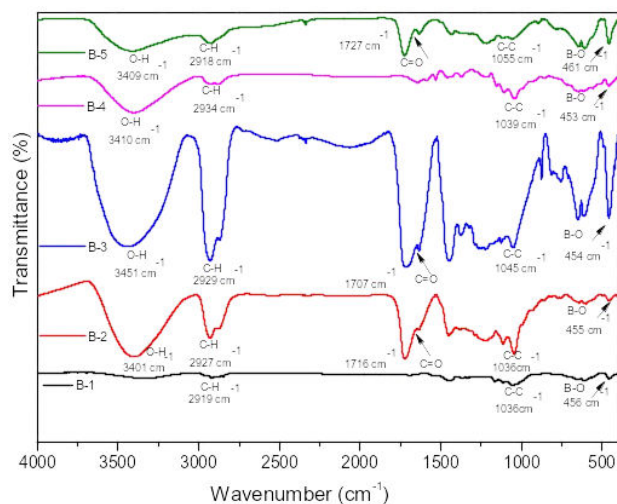


FIGURE 2. FT-IR spectra of the colloidal solutions of samples B-1, B-2, B-3, B-4, and B-5.

4. Results and discussion

4.1. FT-IR spectroscopy

Figure 2 shows the FT-IR spectra of the boron powders (B-1, B-2, B-3, B-4, and B-5). The duality of glycerol as a reducing and encapsulating agent is due to the decomposition of glycerol into primary alcohols, which function as reducers. Additionally, the vibrational bonds of C-C, C-H, and C=O indicate the presence of radicals on the surface of the nanoparticles, which are formed as alkoxides and act as encapsulants, supporting the uniformity of the nanoparticle size.

The band located at approximately 2930 cm^{-1} corresponds to the symmetric stretching vibration of the C-H bond, indicating the presence of -CH₂-OH. The 3400 and 1040 cm^{-1} bands can be attributed to the -OH and C-O vibrational bonds, respectively, indicating glycerol decomposition into primary alcohols. Once the decomposition of glycerol into primary alcohols occurred, a band appeared at approximately 1720 cm^{-1} , corresponding to the C=O vibrational bond, which is associated with glycerol on the surface of the nanoparticles [22]. Finally, the band situated at approximately 450 cm^{-1} is related to the B-O vibrational bond, indicating the formation of boron nanoparticles with an oxide layer on their surface [22-36]. The change in the intensities of the bands is probably due to environmental conditions, the amount of the sample, and the sensibility of equipment for each analysis, as can be observed in spectra B-1 and B-4, where the same bands are presented but with different intensities. In the case of samples B-1 and B-4, it may be due to a variation of the sample analyzed. Another example is the band located at approximately 3400 cm^{-1} is due to the high hygroscopicity of glycerol, which absorbs water molecules from the environment, similar results were obtained by Tianhao Lui *et al.* [22], who synthesized silver nanoparticles using glycerol as a reducing agent, which confirmed the decomposition of glycerol and its role as an encapsulant.

4.2. Structural analysis by X-ray diffraction

The crystalline structure of the boron powders was determined at room temperature using X-ray diffraction (Fig. 3). Although there are four possible crystallographic arrangements of boron (α -rhombohedral, β -rhombohedral, α -tetragonal, and γ -tetragonal), the amorphous form exhibits better thermal properties and is, therefore, preferred as a highly energetic material.

All the samples (B-1, B-2, B-3, B-4, and B-5) exhibit a single broad peak between 11.61° and 28.99°, which is characteristic of amorphous boron [37]. This peak is generally indicative of an amorphous material, although its appearance here is not solely attributable to the presence of amorphous boron [38]. XRD studies of boron nanopowders synthesized by the sol-gel method, as reported by Abolhassan Najafi *et al.* [39], showed a diffraction peak located between 10.5° and 30.5°, associated with boron, carbon, and amorphous oxygen. This behavior occurs due to a change in the pH of the

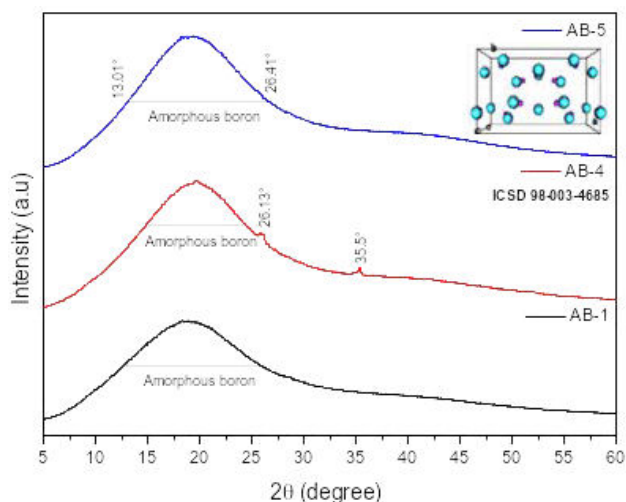


FIGURE 3. X-ray diffraction patterns of the amorphous boron and a secondary boron phase, at high pressure.

sols during condensation and drying under an inert gas [40]. Of the three systems analyzed (AB-1, AB-4, and AB-5), only sample AB-4 exhibits a stable secondary phase of boron to high pressure. This is confirmed by the peaks located at $2\theta = 26.13^\circ$ and 35.5° , which are representative of a high-pressure stable secondary boron phase with an orthorhombic structure (ICSD- 98-003-4685), which can induce the recrystallization of some boron atoms, leading to the formation of crystalline boron with an orthorhombic structure. It is known that amorphous boron possesses excellent mechanical properties; therefore, a secondary phase in such samples can be considered an impurity that affects the hardness, electrical properties, and thermal properties of amorphous boron nanoparticles [41].

4.3. UV-Visible spectroscopy analysis

Figure 4 shows the results of the UV-Vis studies of samples B-1, B-2, and B-3. Two surface plasmon resonance (SPR) bands are observed in all the samples analyzed. The first band is due to the resonance frequency and the width of the plasmon absorption band [42-43]. The second band may be attributed to a change in particle morphology or to the formation of the presence of non-uniform particles. This suggests two plasmonic resonances in different directions in three-dimensional space, which can be verified by microscopy studies. The boron nanoparticles under examination were synthesized using glycerol as a reducing agent, deionized water at two different concentrations (50% and 80% v/v glycerol and water), and boron ions at two concentrations (0.1 M and 0.2 M).

The first band is located around ~ 200 nm, while the second is situated at ≈ 274 nm. The brown and dark brown colors of the solutions signal the presence of boron colloids. Color changes in colloidal solutions are associated with changes in particle size. In colloidal solutions of AgB nanoparticles, Ahmed I. El-Batal *et al.* [44] observed a color

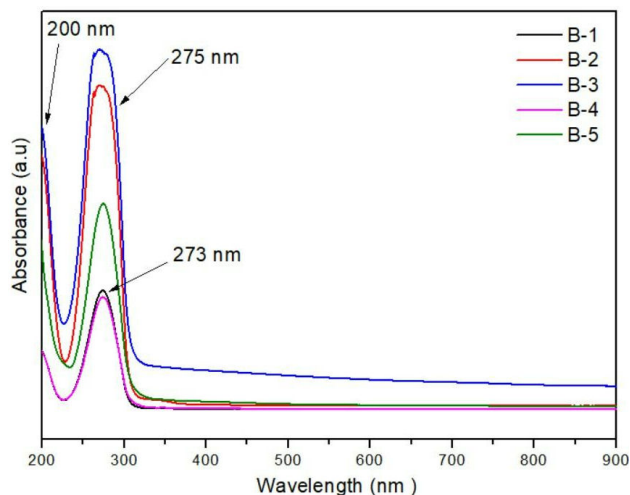


FIGURE 4. Surface plasmon resonance band of the colloidal solutions of boron (B-1, B-2, B-3, B-4 and B-5) at different concentrations of glycerol, metal ions, and encapsulant.

change from brown to dark brown, which was related to particle size. The colloidal solutions obtained presented a surface plasmon band located at ~ 410 nm, indicating the presence of AgB nanoparticles with sizes smaller than 100 nm. These results were confirmed by TEM. The formation of a double or triple band in boron colloids can be attributed to a change in morphology; however, interactions at wavelengths greater than 600 nm suggest that larger particles form, causing agglomerations [45]. In contrast, interactions occurring at shorter wavelengths (400 nm) are associated with the presence of small particles with an approximate size of 50 nm [46]. These require lower amounts of energy for the polariton (electrons in the conduction band) to respond with a single plasmonic resonance band [21].

Figure 5 shows the influence of the encapsulant (PVP) on the boron nanoparticles. Samples B-1 (0.2 M, 80% glycerol, and 0.02 g of PVP) and B-4 (0.2 M., 80% glycerol, and 0.01 g of PVP) display a band located at ~ 274 nm.

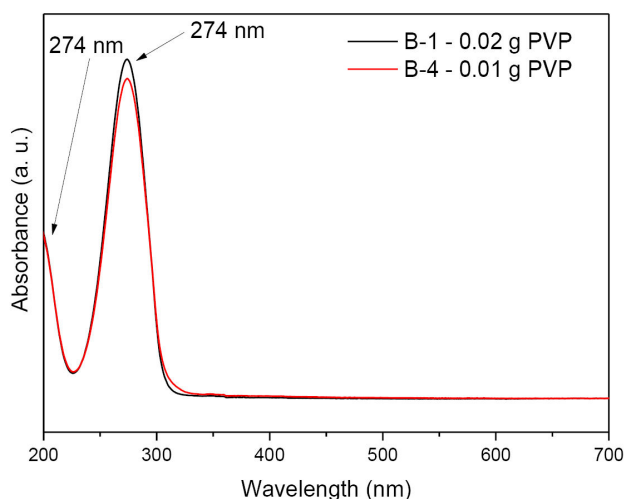


FIGURE 5. Influence of PVP on boron nanoparticles.

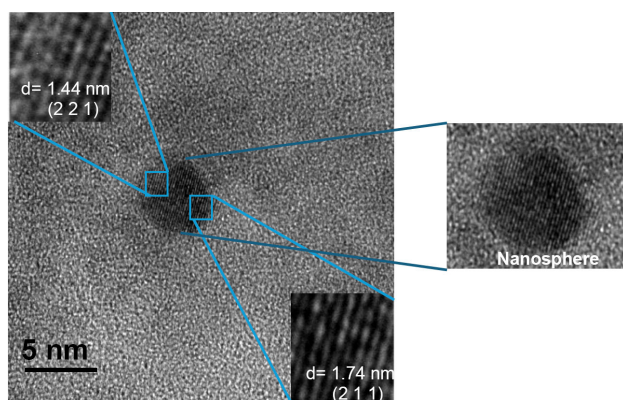


FIGURE 6. TEM micrograph of a boron nanoparticle with a spherical morphology.

An increase in absorbance of 5 units is observed in the surface plasmon resonance band when the concentration of PVP is 0.02 g. These results indicate that the amount of PVP increases the uniformity of the nanoparticles due to greater steric repulsion in the PVP ligands [47]. S. K. Maurya *et al.* [48] studied the influence of PVP concentration on the surface plasmon resonance response in silver nanoparticles. It has been demonstrated that the amount of PVP used as a capping agent in the synthesis of metal nanoparticles modifies the morphology and promotes the uniformity of spherical particles [49-50].

4.4. Morphological studies

4.4.1. Transmission electron microscopy

The Transmission electron microscopy (TEM) micrograph (Fig. 6) of sample B-3 shows a single spherical nanoparticle with a diameter of approximately 5 nm.

This image corroborates the results obtained by SPR. A band located at 273 nm can be seen, characteristic of metal nanoparticles with spherical morphology and sizes smaller than 100 nanometers. The relationship between short wavelengths and the polariton of the boron nanoparticles depends on the size and morphology of the nanoparticles by influencing the quantized energy levels and the overall interaction between light and the electronic excitations in the conduction band of the nanoparticles.

The analysis with high-resolution transmission electron microscopy (HRTEM) shows the crystallographic planes (2 2 1) and (2 2 2), which correspond to interplanar spaces of 1.74 nm and 1.44 nm, respectively. It is important to note that the high-resolution micrograph (Fig. 6) shows particles composed of individual crystallites with characteristics indicative of an orthorhombic structure (ICSD 98-003-4685), which is associated with boron oxide at high pressure [51-52].

4.4.2. Scanning electron microscopy

In the scanning electron microscopy (SEM) micrograph (Fig. 7a), microparticles with spherical and quasi-spherical

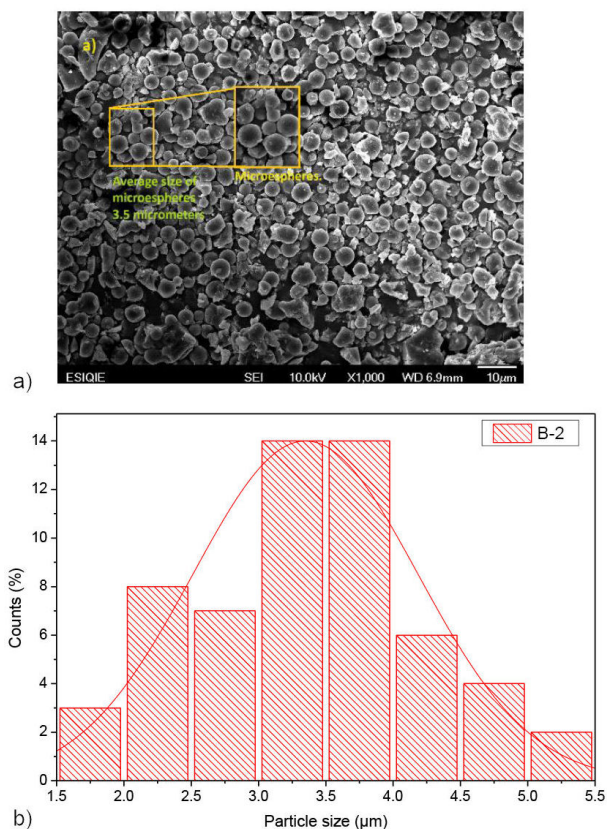


FIGURE 7. a) Scanning electron micrograph and b) distribution histogram of the boron particles.

morphologies are observed, with an approximate size of 3.5 μm , as seen in the histogram [Fig. 7b)], which shows the particle size distribution.

According to the results obtained by SPR and TEM, in which both support the presence of boron nanoparticles, it is possible that the formation of these microparticles is due to the assembling of nanometric particles.

5. Conclusion

In this work, we successfully synthesized boron nanoparticles using a novel hybrid “polyol-solvothermal” method. The presence of the vibrational bonds OH-, C-H, and C=O corroborated the double functionality of glycerol as both a reducer and encapsulant. Microscopy studies revealed that using an encapsulant such as PVP promotes the formation of clusters of nanoparticles with spherical and quasi-spherical morphologies and sizes of approximately 5 nm.

SPR corroborated the obtaining of boron nanoparticles. In all the samples, two plasmonic bands were observed under exposure to short wavelengths (UV), the first at approximately 200 nm and the second at 273 nm. These bands are observed only in metallic and metalloid nanoparticles of nanometric size. Finally, boron nanoparticles synthesized this way show promise for storing significant amounts of energy for fuel applications.

Acknowledgments

The authors gratefully acknowledge the financial support of this work by the Instituto Politécnico Nacional through SIP-IPN projects 20241486 and 20241489. A. Casas Mendoza acknowledges the Conahcyt Ph.D. scholarship. The authors

thank CNMN-IPN, Lab CREA-CIITEC IPN, UPIITA IPN, and ESIIQIE IPN for their experimental support. The authors also would like to thank Henry Jankiewicz for the editing work he did for this paper and M. García Murillo for her assistance.

- I. Khan, K. Saeed, and I. Khan, Nanoparticles: Properties, applications and toxicities, *Arabian Journal of Chemistry*, **12** (2019) 908, <https://doi.org/10.1016/J.ARABJC.2017.05.011>.
- N. Narayan, A. Meiyazhagan, and R. Vajtai, Metal Nanoparticles as Green Catalysts, *Materials* **12** (2019) 3602, <https://doi.org/10.3390/MA12213602>.
- H. W. Tan, J. An, C. K. Chua, and T. Tran, Metallic Nanoparticle Inks for 3D Printing of Electronics, *Adv. Electron. Mater.* **5** (2019) 1800831, <https://doi.org/10.1002/AELM.201800831>.
- M. D. Nguyen, H. V. Tran, S. Xu, and T. R. Lee, Fe₃O₄ Nanoparticles: Structures, Synthesis, Magnetic Properties, Surface Functionalization, and Emerging Applications, *Applied Sciences*, **11** (2021) 11301, <https://doi.org/10.3390/APP112311301>.
- O. Matátková, J. Michailidu, A. Miškovská, I. Kolouchová, J. Masák, and A. Čejková, Antimicrobial properties and applications of metal nanoparticles biosynthesized by green methods, *Biotechnol. Adv.* **58** (2022) 107905, <https://doi.org/10.1016/J.BIOTECHADV.2022.107905>.
- X. Cheng, Tuning metal catalysts via nitrogen-doped nanocarbons for energy chemistry: From metal nanoparticles to single metal sites, *Energy Chem*, **3** (2021) 100066, <https://doi.org/10.1016/J.ENCHEM.2021.100066>.
- J. P. Scheifers, Y. Zhang, and B. P. T. Fokwa, Boron: Enabling Exciting Metal-Rich Structures and Magnetic Properties, *Acc Chem Res*, **50** (2017) 2317, <https://doi.org/10.1021/ACS.ACCOUNTS.7B00268>.
- P. Govindrao Jamkhande, N. W. Ghule, A. Haque Bamer, and M. G. Kalaskar, Metal nanoparticles synthesis: An overview on methods of preparation, advantages and disadvantages, and applications, *Journal of Drug Delivery Science and Technology* **53** (2019) 101174, <https://doi.org/10.1016/j.jddst.2019.101174>.
- A. Banisharif, P. Estellé, A. Rashidi, S. Van Vaerenbergh, and M. Aghajani, Heat transfer properties of metal, metal oxides, and carbon water-based nanofluids in the ethanol condensation process, *Colloids Surf A Physicochem Eng Asp*, **622** (2021) 126720, <https://doi.org/10.1016/J.COLSURFA.2021.126720>.
- Z. Lin, Rapid synthesis of metallic and alloy micro/nanoparticles by laser ablation towards water, *Appl. Surf. Sci.* **504** (2020) 144461, <https://doi.org/10.1016/J.APSUSC.2019.144461>.
- K. Kavitha, T. Subba Rao, and R. Padma Suvarna, Synthesis and characterization of ZnO-CuO nanocomposites, *AIP Conf. Proc.*, **2269** (2020) 030078, <https://doi.org/10.1063/5.0019509/724014>.
- S. Kamrani, D. Penther, A. Ghasemi, R. Riedel, and C. Fleck, Microstructural characterization of Mg-SiC nanocomposite synthesized by high energy ball milling, *Advanced Powder Technology*, **29** (2018) 1742, <https://doi.org/10.1016/J.APT.2018.04.009>.
- K. Parveen, V. Banse, and L. Ledwani, Green synthesis of nanoparticles: Their advantages and disadvantages, *AIP Conf Proc*, **1724** (2016) 020048, <https://doi.org/10.1063/1.4945168>.
- D. Zhang, X. L. Ma, Y. Gu, H. Huang, and G. W. Zhang, Green Synthesis of Metallic Nanoparticles and Their Potential Applications to Treat Cancer, *Front Chem*, **8** (2020) <https://doi.org/10.3389/FCHEM.2020.00799>.
- L. Y. Meng, B. Wang, M. G. Ma, and K. L. Lin, The progress of microwave-assisted hydrothermal method in the synthesis of functional nanomaterials, *Mater Today Chem*, **1-2** (2016) 63, <https://doi.org/10.1016/J.MTCHEM.2016.11.003>.
- M. Parashar, V. K. Shukla, and R. Singh, Metal oxides nanoparticles via sol-gel method: a review on synthesis, characterization and applications, *Journal of Materials Science: Materials in Electronics*, **31** (2020) 3729, <https://doi.org/10.1007/S10854-020-02994-8>.
- L. P. Faden *et al.*, Sc, Zr, Hf, and Mn Metal Nanoparticles: Reactive Starting Materials for Synthesis Near Room Temperature, *Inorg Chem*, **63** (2024) 1020, <https://doi.org/10.1021/ACS.INORGCHEM.3C03074>.
- O. Ogunkunle and N. A. Ahmed, A review of global current scenario of biodiesel adoption and combustion in vehicular diesel engines, *Energy Reports*, **5** (2019) 1560, <https://doi.org/10.1016/j.egyr.2019.10.028>.
- J. Kou, C. Bennett-Stamper, and R. S. Varma, Green synthesis of noble nanometals (Au, Pt, Pd) using glycerol under microwave irradiation conditions, *ACS Sustain Chem Eng*, **1** (2013) 810, <https://doi.org/10.1021/SC400007P>.
- R. Govindaraju, S. S. Chen, L. P. Wang, H. M. Chang, and M. Pasawan, Significance of Membrane Applications for High-Quality Biodiesel and Byproduct (Glycerol) in Biofuel Industries-Review, *Curr Pollut Rep*, **7** (2021) 128, <https://doi.org/10.1007/S40726-021-00182-8>.
- R. Parveen, S. Ullah, R. Sgarbi, and G. Tremiliosi-Filho, One-pot ligand-free synthesis of gold nanoparticles: The role of glycerol as reducing-cum-stabilizing agent, *Colloids Surf a Physicochem Eng Asp*, **565** (2019) 162, <https://doi.org/10.1016/J.COLSURFA.2019.01.005>.

22. T. Liu, D. R. Baek, J. S. Kim, S. W. Joo, and J. K. Lim, Green Synthesis of Silver Nanoparticles with Size Distribution Depending on Reducing Species in Glycerol at Ambient pH and Temperatures, *ACS Omega*, **5** (2020) 16246, <https://doi.org/10.1021/ACSOMEGA.0C02066>.
23. A. F. Cristino, I. A. S. Matias, D. E. N. Bastos, R. Galhano dos Santos, A. P. C. Ribeiro, and L. M. D. R. S. Martins, Glycerol Role in Nano Oxides Synthesis and Catalysis, *Catalysts* **10** (2020) 1406, <https://doi.org/10.3390/catal10121406>.
24. G. Habibullah, J. Viktorova, and T. Ruml, Current strategies for noble metal nanoparticle synthesis. *Nanoscale Research Letters*, **16** (2021) 47, <https://doi.org/10.1186/s11671-021-03480-8>.
25. A. Demirbas, E. Kislakci, Z. Karaagac, I. Onal, N. Ildiz, and I. Ocoy, Preparation of biocompatible and stable iron oxide nanoparticles using anthocyanin integrated hydrothermal method and their antimicrobial and antioxidant properties, *Mater Res Express*, **6** (2019) 125011, <https://doi.org/10.1088/2053-1591/AB540C>.
26. T. A. Taha, A. A. Azab, and M. A. Sebak, Glycerol-assisted sol-gel synthesis, optical, and magnetic properties of NiFe₂O₄ nanoparticles, *J. Mol. Struct.*, **1181** (2019) 14, <https://doi.org/10.1016/J.MOLSTRUC.2018.12.075>.
27. A. Nirmala Grace and K. Pandian, One pot synthesis of polymer protected Pt, Pd, Ag and Ru nanoparticles and nanoprisms under reflux and microwave mode of heating in glycerol-A comparative study, *Mater Chem. Phys.* **104** (2007) 191, <https://doi.org/10.1016/J.MATCHEMPHYS.2007.03.009>.
28. H. Chen *et al.*, Construction of a Nanoporous Highly Crystalline Hexagonal Boron Nitride from an Amorphous Precursor for Catalytic Dehydrogenation, *Angewandte Chemie*, **131** (2019) 10736, <https://doi.org/10.1002/ANGE.201904996>.
29. F. Lu *et al.*, Polypyrrole-functionalized boron nitride nanosheets for high-performance anti-corrosion composite coating, *Surf. Coat. Technol.* **420** (2021) 127273, <https://doi.org/10.1016/J.SURFCOAT.2021.127273>.
30. I. D. Giovannelli-Maizo, A. P. Luz, and V. C. Pandolfelli, Advanced boron-containing refractory castables bonded with calcium-free binders, *Ceram. Int.* **45** (2019) 8774, <https://doi.org/10.1016/J.CERAMINT.2019.01.202>.
31. M. Li *et al.*, Highly thermal conductive and electrical insulating polymer composites with boron nitride, *Compos. B. Eng.*, **184** (2020) 107746, <https://doi.org/10.1016/J.COMPOSITESB.2020.107746>.
32. S. Huang, S. Deng, Y. Jiang, and X. Zheng, Experimental effective metal oxides to enhance boron combustion, *Combust Flame*, **205** (2019) 278, <https://doi.org/10.1016/J.COMBUSTFLAME.2019.04.018>.
33. J. M. Maita, G. Song, M. Colby, and S. W. Lee, Atomic arrangement and mechanical properties of chemical-vapor-deposited amorphous boron, *Mater Des.*, **193** (2020) 108856, <https://doi.org/10.1016/J.MATDES.2020.108856>.
34. A. Alrebh and J. L. Meunier, Synthesis of boron nitride nanosheets powders using a plasma based bottom-up approach, *2d Mater.* **8** (2021) 045018, <https://doi.org/10.1088/2053-1583/AC1854>.
35. T. Xu *et al.*, Advances in synthesis and applications of boron nitride nanotubes: A review, *Chemical Engineering Journal*, **431** (2022) 134118, <https://doi.org/10.1016/J.CEJ.2021.134118>.
36. T. Liu, D. R. Baek, J. S. Kim, S. W. Joo, and J. K. Lim, Green Synthesis of Silver Nanoparticles with Size Distribution Depending on Reducing Species in Glycerol at Ambient pH and Temperatures, *ACS Omega*, **5** (2020) 16246, <https://doi.org/10.1021/ACSOMEGA.0C02066/ASSET/IMAGES/LARGE/AO0C02066.0010.JPEG>.
37. Z. H. Dou, T. A. Zhang, G. Y. Shi, C. Peng, M. Wen, and J. C. He, Preparation and characterization of amorphous boron powder with high activity, *Transactions of Nonferrous Metals Society of China* **24** (2014) 1446, [https://doi.org/10.1016/S1003-6326\(14\)63211-8](https://doi.org/10.1016/S1003-6326(14)63211-8).
38. Z. H. Dou, T. A. Zhang, J. C. He, and Y. Huang, Preparation of amorphous nano-boron powder with high activity by combustion synthesis, *J. Cent. South. Univ.*, **21** (2014) 9, <https://doi.org/10.1007/S11771-014-2016-2>.
39. A. Najafi, F. Golestani-Fard, H. R. Rezaie, and S. P. Saeb, Sol-Gel synthesis and characterization of SiC-B₄C nano powder, *Ceram Int.* **47** (2021) 6376, <https://doi.org/10.1016/J.CERAMINT.2020.10.218>.
40. M. Giuseppe *et al.*, Pressureless sintering and properties of α -SiC-B₄C composite. *Journal of the European Ceramic Society*, **21** (2023) 633, [https://doi.org/10.1016/S0955-2219\(00\)00244-2](https://doi.org/10.1016/S0955-2219(00)00244-2),
41. E. F. M. El-Zaidia *et al.*, Effect of film thickness on structural, electrical and optical properties of amorphous boron subphthalocyanine chloride thin film, *Opt. Mater (Amst)*, **138** (2023) 113691, <https://doi.org/10.1016/J.OPTMAT.2023.113691>.
42. L. Cornejo, Resonancia del plasmón de la superficie (RPS). Accessed: Mar. 19, (2024), <https://nuevatecnologiasymateriales.com/resonanciadel-plasmon-de-la-superficie-rps-propiedades-optoelectronicas/>
43. Available: <https://nuevatecnologiasymateriales.com/resonanciadel-plasmon-de-la-superficie-rps-propiedades-optoelectronicas/>
44. S. A. Lee and S. Link, Chemical Interface Damping of Surface Plasmon Resonances, *Acc Chem Res*, **54** (2021) 1950, <https://doi.org/10.1021/ACS.ACCOUNTS.0C00872>.
45. A. I. El-Batal, G. S. El-Sayyad, N. E. Al-Hazmi, and M. Gobara, Antibiofilm and Antimicrobial Activities of Silver Boron Nanoparticles Synthesized by PVP Polymer and Gamma Rays Against Urinary Tract Pathogens, *J Clust Sci*, **30** (2019) 947, <https://doi.org/10.1007/S10876-019-01553-4>.
46. S. A. Uspenskii *et al.*, Russian Text The Author(s), *Doklady Chemistry*, **491** (2020) 20, <https://doi.org/10.1134/S0012500820030027>.

47. A. I. El-Batal, M. S. Attia, M. M. Nofel, and G. S. El-Sayyad, Potential Nematicidal Properties of Silver Boron Nanoparticles: Synthesis, Characterization, In Vitro and In Vivo Root-Knot Nematode (*Meloidogyne incognita*) Treatments, *J. Clust. Sci.*, **30** (2019) 687, <https://doi.org/10.1007/S10876-019-01528-5>.
48. K. Seo, K. Sinha, E. Novitskaya, and O. A. Graeve, Polyvinylpyrrolidone (PVP) effects on iron oxide nanoparticle formation, *Mater Lett*, **215** (2018) 203, <https://doi.org/10.1016/J.MATLET.2017.12.107>.
49. S. K. Maurya, R. A. Ganeev, A. Rout, and C. Guo, Influence of PVP polymer concentration on nonlinear absorption in silver nanoparticles at resonant excitation, *Appl Phys A Mater Sci Process*, **126** (2020) 1, <https://doi.org/10.1007/S00339-019-3208-2/FIGURES/5>.
50. T. Song *et al.*, A review of the role and mechanism of surfactants in the morphology control of metal nanoparticles, *Nanoscale*, **13** (2021) 3895, <https://doi.org/10.1039/D0NR07339C>.
51. I. A. Safo, M. Werheid, C. Dosche, and M. Oezaslan, The role of polyvinylpyrrolidone (PVP) as a capping and structure-directing agent in the formation of Pt nanocubes, *Nanoscale Adv*, **1** (2019) 3095, <https://doi.org/10.1039/C9NA00186G>.
52. N. Aliyeva, T. C. Canak, and İ. E. Serhatlı, Synthesis and characterization of boron-acrylate/Santa Barbara Amorphous-15 polymer composite, *J. Appl. Polym. Sci.*, **138** (2021) 50445 <https://doi.org/10.1002/APP.50445>.
53. P. Saravanan, K. SenthilKannan, R. Divya, M. Vimalan, S. Tamilselvan, and D. Sankar, A perspective approach towards appreciable size and cost-effective solar cell fabrication by synthesizing ZnO nanoparticles from *Azadirachta indica* leaves extract using domestic microwave oven, *J. Mater. Science: Materials in Electronics*, **31** (2020) 4301, <https://doi.org/10.1007/S10854-020-02985-9>.